Indium-111-Chloride and Three-Phase Bone Scintigraphy: A Comparison for Imaging Experimental Osteomyelitis

James J. Hoskinson, Gregory B. Daniel, and Clark S. Patton

Radiology Section, Department of Urban Practice and Department of Pathobiology, University of Tennessee College of Veterinary Medicine, Knoxville, Tennessee

To investigate the utility of indium-111-chloride (^{111}In-Cl) imaging in detecting osteomyelitis complicating surgical or fracture sites, the proximal tibia of 11 dogs were experimentally infected with *Staphylococcus aureus* after creation of a cortical defect. The contralateral limb served as a sham-operated control. Animals were serially imaged by radiography, three-phase technetium-99m-methylene diphosphonate (^{99m}Tc-MDP) scintigraphy, and ^{111}In-Cl scintigraphy. There was a significant difference between infected (1.93) and noninfected (1.32) limb's tibia/femur count density ratios on 24-hr ($p = 0.0001$) and 72-hr ($p = 0.0001$) ^{111}In-Cl images. A smaller difference was found for ^{99m}Tc-MDP bone-phase tibia/femur ratios ($p = 0.0199$). Using receiver operator characteristic analysis of tibia/femur ratios, a sensitivity of 61%, specificity of 88%, and positive (75%) and negative (79%) predictive values were determined for the 24-hr ^{111}In-Cl images. Indium-111-chloride was superior to ^{99m}Tc-MDP in differentiating infected and noninfected operative sites.

J Nucl Med 1991; 32:67–75

It is frequently difficult to obtain an early diagnosis of osteomyelitis. Early detection may influence patient management, improve therapeutic response, and identify areas of clinical interest for biopsy or monitoring (*1–3*).

Current modalities for imaging osteomyelitis include radiography (*3,4*), computed tomography (*3*), technetium-99m-methylene diphosphonate (^{99m}Tc-MDP) bone scanning (*3,5–16*), gallium-67-citrate scanning (*5, 7–14,16,17*), radiolabeled (^{111}In, ^{99m}Tc) leukocyte scanning (*4,8,9,13,18*), and magnetic resonance imaging (*12,17*). While advances have been made in imaging bone infection, problems associated with each of these techniques remain.

Indium-111-chloride (^{111}In-Cl) has shown a greater than 90% sensitivity in detecting acute (*18*) and chronic (*19*) osteomyelitis in human patients with a high degree of specificity (*18–21*). Because of ^{111}In-Cl's uptake by erythropoietic tissue (*22–24*), bone grafts or biopsy sites that displace erythroid marrow may cause false-positives (*19*). With these exceptions, ^{111}In-Cl does not label in the absence of inflammation (*19*); therefore, ^{111}In-Cl may be of value in detecting infection in healing fractures.

While ^{111}In-Cl has been used for some time as an erythroid marrow imaging agent (*22,23*), its use for imaging inflammatory disease has been limited. Clinical reports have appeared (*18–20,24,25*), but no controlled studies have been performed to evaluate its use as an inflammatory imaging agent. This project was designed to evaluate the sensitivity and specificity of ^{111}In-Cl for imaging osteomyelitis after bone trauma in a dog model.

MATERIALS AND METHODS

Radiopharmaceuticals

Technetium-99m-MDP was prepared from a commercially available kit. Carrier-free ^{111}In-Cl at an acid pH was obtained from New England Nuclear, North Billerica, MA or Amersham, Arlington Heights, IL.

Staphylococcus aureus Suspension

A *S. aureus* suspension was prepared from a frozen canine osteomyelitis isolate. The organism was grown in trypticase soy broth and suspended in saline to achieve a spectrophotometrically determined concentration of 5×10^7 organisms/ml.

Experimental Animals

Eleven preconditioned, healthy dogs were used. All dogs had normal skeletons, were over 18 mo of age, and weighed 12–20 kg. All procedures and treatment protocols were performed under American Association for Accreditation of Laboratory Animal Care (AAALAC) guidelines with approval of

Received Feb. 20, 1990; revision accepted Jul. 19, 1990.

For reprints contact: James J. Hoskinson, Dept. of Radiological Sciences, Univ. of Calif.-Davis School of Veterinary Medicine, Davis, CA 95616.

the University of Tennessee Animal Care and Concerns Committee.

Creation of Osteomyelitis

Animals were preanesthetized with acepromazine (2 mg s.c.) and atropine (0.04 mg/kg s.c.). Anesthesia was induced with i.v. thyamylal sodium and maintained with a halothane/oxygen mix by inhalation. After exposing the craniomedial aspect of the proximal tibial metaphysis of both limbs, a cortical defect was made in each tibia with a 9.5-mm Steinmann pin. A small piece of sterile saline-soaked cotton was introduced into the medullary cavity of each tibia. One-half milliliter of the *S. aureus* suspension (~2.5×10^7 organisms) was injected into the cotton in one tibia of each dog. The opposite limb served as a sham-operated control. The fascia and skin were closed with a monofilament absorbable suture.

Imaging

Each animal was imaged preoperatively and at 5, 14, and 23 days postoperatively. Craniocaudal and mediolateral survey radiographs were made of each tibia. Following radiographs, three-phase ^{99m}Tc-MDP bone scans were performed. A dynamic acquisition (64 × 64 matrix) was made at 3 sec per frame for 60 sec. Static images were acquired for 250,000 counts, and the acquisition time was recorded.

At the conclusion of ^{99m}Tc-MDP imaging, the animals were injected intravenously with 750–1000 μCi (27–37 MBq) of ^{111}In-Cl. All ^{111}In-Cl images were made using a medium-energy collimator and 15% windows centered at the 173 and 247 keV photopeaks (*18,19*). At 24 hr postinjection, 5-min acquisition images were made of both limbs (cranial and lateral views). At 72 hr after injection, a second acquisition was made for 10 min. The animals were immobilized during image acquisition with i.v. acepromazine, diazepam, and ketamine.

Postmortem Evaluation

The animals were euthanized on the twenty-sixth postoperative day. Swabs of the bone surface were submitted for aerobic and anaerobic culture. A 1-cm wide transverse section of the tibia including the implant site was removed and fixed in 10% buffered neutral formalin. Bone samples were decalcified in citrate-buffered formic acid, imbedded in paraffin, and sectioned at 5 microns. Hematoxylin/eosin and gram-stained sections were examined for confirmation or exclusion of osteomyelitis. A diagnosis of infection was made based on culture and histology findings.

Data Analysis

Radiographs were graded by two veterinary radiologists (JJH, GBD) individually according to the following system:

Grade 0. No radiographic abnormalities other than the iatrogenic cortical defect.
Grade 1. Soft-tissue swelling at the operative site, no bony lesion.
Grade 2. ± soft-tissue swelling, irregular periosteal reaction limited to <2 cm from the cortical defect.
Grade 3. Irregular periosteal reaction extending >2 cm from cortical defect and/or evidence of cortical lysis adjacent to defect.
Grade 4. Extensive cortical destruction.

Films were presented randomly without prior knowledge of patient identification, time relative to surgery, or infected versus noninfected limb. In the few cases where there was not agreement, the film was reviewed jointly and a final grade assigned.

Technetium-99m-MDP angiogram images were evaluated by each reader and assigned to one of three categories: increased initial activity in the right limb, increased initial activity in the left limb, or equal activity. Soft-tissue phase images were similarly categorized based on relative intensity in the proximal tibia. Additionally, the relative intensity of the tibia versus femur and of the medial proximal tibia versus soft tissue of the thigh were categorized as of equal, greater, or lesser intensity.

For the ^{99m}Tc-MDP bone-phase and ^{111}In-Cl images, count density per minute (counts/pixel/min) was calculated by placing equal sized square regions of interest over the distal femur, proximal tibia, and soft tissues of the thigh (Fig. 1). A slightly smaller square region was used for the distal tibia to exclude pixels outside bone margins.

A multiple variable analysis of repeated measure was performed on a computerized statistical program (Solo, BMDP Statistical Software, Los Angeles, CA). The interaction of the individual, the treatment, the view and the day of imaging, and all combinations of these were analyzed. A paired t-test was used to compare infected and noninfected ratios.

The following ratios were also calculated and compared using paired t-tests for each imaging day and all days grouped together.

$$\text{Inf/Noninf ratio} = \frac{\text{Tibia/femur ratio (infected limb)}}{\text{Tibia/femur ratio (noninfected limb)}}$$

$$\text{In-Cl/Tc-MDP ratio} = \frac{\text{Tibia/femur ratio } (^{111}\text{In-Cl})}{\text{Tibia/femur ratio } (^{99m}\text{Tc-MDP})}$$

Receiver operator characteristic (ROC) curves for postoperative tibia/femur ratios were used to select the optimal cutoff value for determining the sensitivity, specificity, and positive and negative predictive values for ^{99m}Tc-MDP, 24-hr ^{111}In-Cl, and 72-hr ^{111}In-Cl. Values were also calculated for ^{99m}Tc-MDP bone-phase tibia-to-soft tissue, and 72-hr ^{111}In-Cl proximal tibia-to-distal tibia and tibia-to-soft tissue ratios.

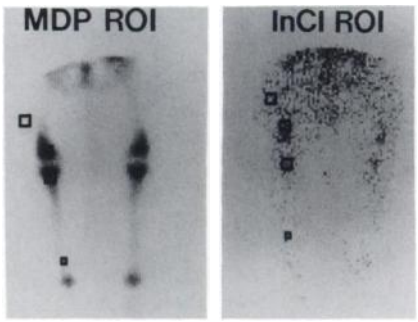

FIGURE 1
Cranial bone-phase ^{99m}Tc-MDP (left) and 24-hr ^{111}In-Cl (right) images with regions of interest displayed. Regions correspond to distal femur, proximal tibia, distal tibia, and soft tissue of the thigh.

TABLE 1
Mean Radiographic Scores and Tibia/Femur Ratios

	Infected				Noninfected			
	Rad	Tc-MDP	24 hr In-Cl	72 hr In-Cl	Rad	Tc-MDP	24 hr In-Cl	72 hr In-Cl
Preop	—	—	—	—	0.00	0.81	0.77	—
Day 5	1.09	1.47	1.78	1.90	1.91	1.19	1.32	1.26
Day 14	2.73	2.75	2.18	2.39	1.64	2.62	1.46	1.52
Day 23	3.45	2.35	1.83	1.83	1.91	1.84	1.18	1.11
Postop average	2.42	2.19	1.93	2.04	1.82	1.88	1.32	1.30

RESULTS

All eleven animals became infected in only one limb as confirmed by histology and isolation of *S. aureus* from the surgical site. Three animals had a second organism cultured from their infected limb in addition to the *S. aureus*. None of the control limbs became infected, although 81% (9/11) had histologic evidence of a foreign body reaction.

All animals were radiographically normal preoperatively. Using the grading criteria, radiographs were a poor predictor of infection ($p = 0.08$). However, there was a progression of disease over the course of the study (Table 1). There was a difference between infected and noninfected limbs when analyzed by postoperative Day 23 ($p < 0.05$).

Due to the great variation in normal preoperative animals, radionuclide angiograms were unreliable in identifying infection in this experiment.

On preoperative ^{99m}Tc-MDP blood-pool images, all dogs had a normal symmetrical, uniform distribution of activity (Fig. 2). The results of ^{99m}Tc-MDP blood-pool images are summarized in Table 2.

Preoperatively, no difference was found between subsequently infected and noninfected limbs for the ^{99m}Tc-MDP bone-phase or ^{111}In-Cl images (Fig. 2). There was not a significant effect of view (cranial versus lateral) on any preoperative or postoperative ratio. The postoperative ^{99m}Tc-MDP bone-phase tibia-to-femur (T/F) ratios were different ($p = 0.019$) for the infected (mean = 2.19) and noninfected (mean = 1.88) groups (Fig. 3). Technetium-99m-MDP bone-phase tibia-to-soft tissue ratios were also different ($p < 0.005$) for infected and noninfected limbs (Fig. 4). No difference was found between groups for ^{99m}Tc-MDP bone-phase proximal

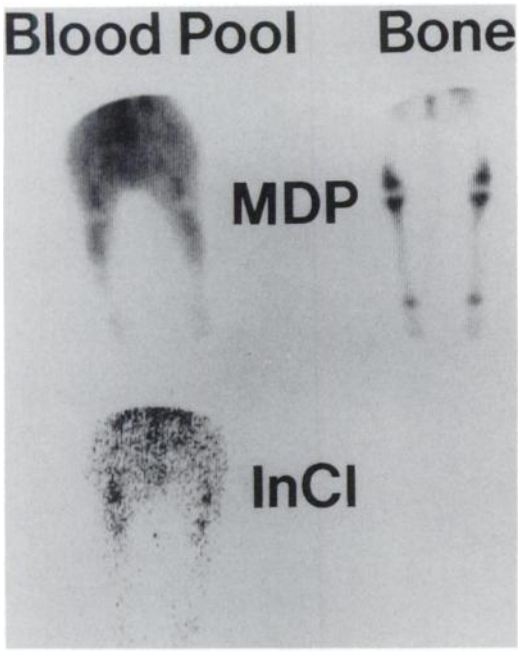

FIGURE 2
Cranial ^{99m}Tc-MDP and ^{111}In-Cl images, preoperative. (Upper left) Normal preoperative blood pool. (Upper right) Bone-phase images. Images are bilaterally symmetrical with normal uptake noted on bone images. (Lower left) Normal preoperative ^{111}In-Cl image shows minimal uptake in the tibia. Erythroid marrow in the distal femur is identified.

TABLE 2
Technetium-99m-MDP Blood-Pool Phase Images

	Preoperative	Postoperative	
Overall limb activity			
inf = noninf	31 (100%)	7 (23%)	
inf > noninf	—	23 (74%)	
inf < noninf	—	1 (3%)	
		Noninfected	Infected
Tibia vs. femur activity			
tibia = femur	31 (100%)	11 (35%)	—
tibia > femur	—	19 (61%)	31 (100%)
tibia < femur	—	1 (3%)	—
Tibia vs. soft-tissue activity			
tibia = soft-tissue	31 (100%)	4 (13%)	16 (52%)
tibia > soft tissue	—	27 (87%)	15 (48%)
tibia < soft tissue	—	—	—

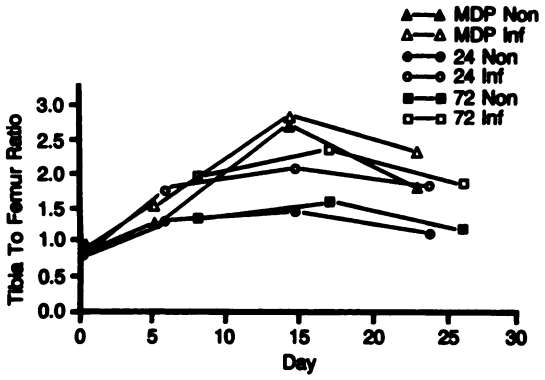

FIGURE 3
Tibia-to-femur ratios for ^{99m}Tc-MDP and ^{111}In-Cl images. Counts/pixel/minute were determined for the operative site and the distal femur on cranial and lateral images. Data points represent means (n = 22).

tibia-to-distal tibia ($p > 0.297$) or femur-to-soft tissue ($p > 0.05$) ratios.

There was a significant difference between infected and noninfected postoperative T/F ratios for both the 24-hr ($p = 0.0001$) and 72-hr ($p = 0.0001$) ^{111}In-Cl images (Figs. 4–5). The mean T/F values for infected and noninfected 24-hr images were 1.93 and 1.32, respectively. The 72-hr mean T/F values were 2.04 and 1.30, respectively. Differences between the 24-hr and 72-hr ^{111}In-Cl T/F ratios for infected ($p = 0.144$) and noninfected ($p = 0.639$) limbs were not significant (Fig. 6). The 24-hr ^{111}In-Cl proximal tibia-to-distal tibia ($p > 0.06$), femur-to-soft tissue ($p > 0.81$), and tibia-to-soft tissue ($p > 0.13$) ratios were not significantly different for infected and noninfected limbs. The difference between 72-hr ^{111}In-Cl proximal tibia-to-distal tibia ($p < 0.035$) and tibia-to-soft tissue ($p < 0.04$) ratios were significant. Table 3 summarizes the infected and noninfected postoperative means along with their level of significance.

When all postoperative images were considered, the mean infected/noninfected ratio for ^{99m}Tc-MDP, 24-

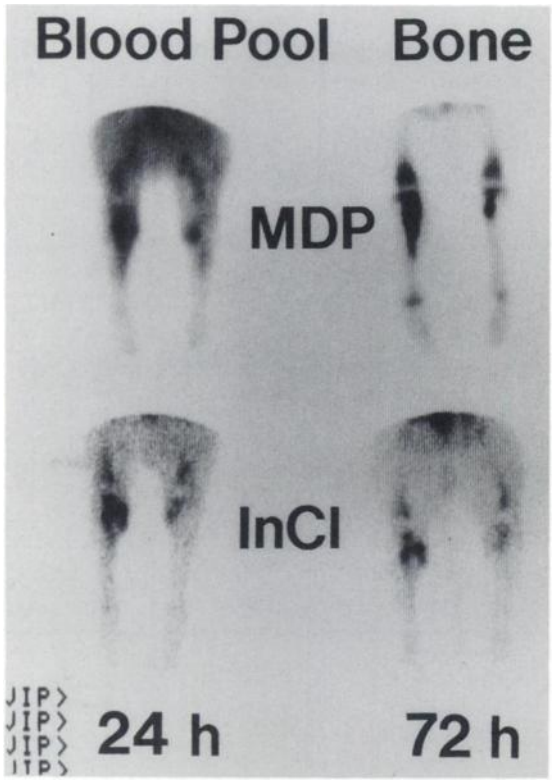

FIGURE 4
Cranial ^{99m}Tc-MDP and ^{111}In-Cl images, Day 14 (same dog as Fig. 2). (Upper left) ^{99m}Tc-MDP blood-pool image demonstrates hyperemia of the infected right limb. There is focal intense uptake in the infected bone and the soft tissues at each skin incision. (Upper right) There is intense uptake on bone-phase images in the proximal half of the right tibia and at the operative site on the left. (Lower left) 24-hr ^{111}In-Cl and (lower right) 72-hr ^{111}In-Cl images have increased uptake in both proximal tibias and in the soft tissue medial to the bone. The uptake is greater in the infected limb at both the bone lesion and soft-tissue site (which was an abscess).

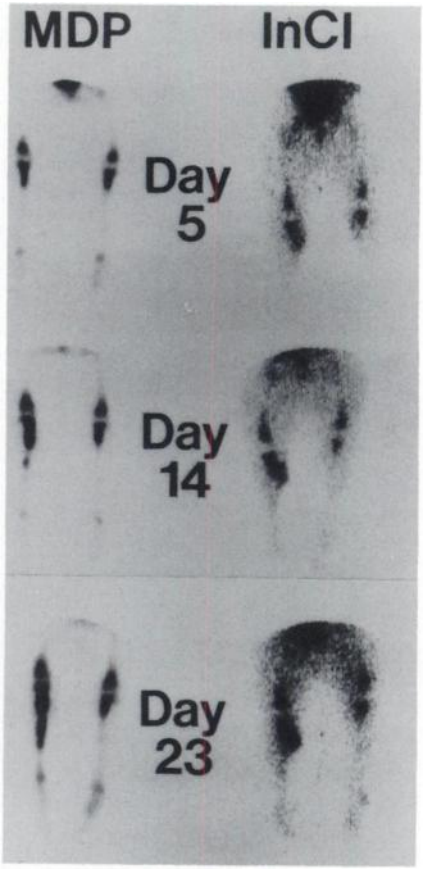

FIGURE 5
Cranial ^{99m}Tc-MDP bone-phase and ^{111}In-Cl images at Days 5, 14, and 23. Day 5: ^{99m}Tc-MDP images are bilaterally symmetrical but ^{111}In-Cl images already show increased uptake in the infected right limb. Faint ^{111}In-Cl uptake is present in the opposite tibia and soft tissues at the incision sites. Day 14: ^{99m}Tc-MDP images have bilateral uptake of similar intensity, although it is more extensive in the infected limb. There is intense ^{111}In-Cl uptake in the proximal tibia and soft tissues medially where a draining tract had formed. Day 23: Images show extensive ^{99m}Tc-MDP uptake in the proximal two-thirds of the right tibia. Indium-111-Cl uptake persists at the site of bone infection and adjacent soft tissues.

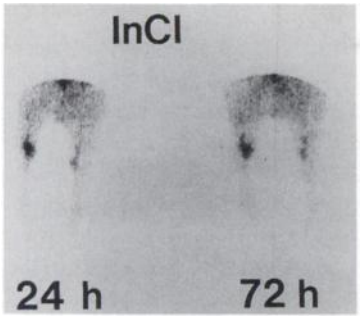

FIGURE 6
Cranial ^{111}In-Cl images, Day 5. Twenty-four and 72-hr ^{111}In-Cl images show an identical pattern of distribution. A slight improvement in target-to-background contrast is appreciated on 72-hr images.

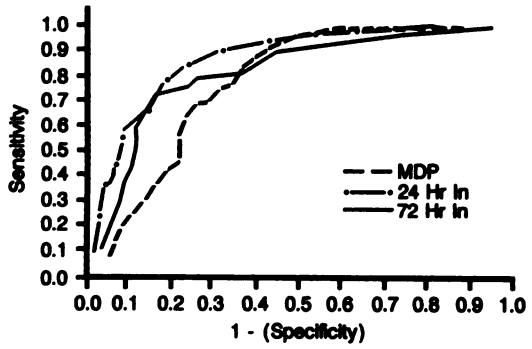

FIGURE 7
Receiver operator characteristic curves for ^{99m}Tc-MDP, 24-hr ^{111}In-Cl, and 72-hr ^{111}In-Cl tibia-to-femur ratios. The optimal cutoff value for ^{99m}Tc-MDP was 1.7. For both 24- and 72-hr ^{111}In-Cl images, the optimal cutoff value was 1.6.

hr, and 72-hr ^{111}In-Cl images were 1.31, 1.52, and 1.62, respectively. The mean In-Cl/Tc-MDP ratios for infected and noninfected limbs at 24 hr were 0.66 and 0.8, respectively, and at 72 hr were 0.62 and 0.82, respectively. Tables 4 and 5 summarize the mean values for these ratios and their significance levels.

Using the ROC curve-derived cutoff T/F ratio of 1.6, sensitivities of 61% and 59%, specificities of 88% and 88%, positive predictive values of 75% and 83%, and negative predictive values of 79% and 68% were calculated for 24-hr and 72-hr ^{111}In-Cl images, respectively. These values are summarized in Table 6.

DISCUSSION

Osteomyelitis represents a diagnostic and therapeutic challenge. Its manifestations are varied and depend on the etiologic agent, the inciting event, the involved site, and the duration of disease (*2,3,13*). The usual presenting signs are pain, limb dysfunction, local swelling, discharge, or systemic signs (fever, malaise). Infection early after internal fixation can be hard to diagnose because pain is often the only clinical finding. Postsurgical complications leading to pain include loose implants, unstable repair, fracture around the implant, hematoma formation, as well as infection (*8,21*). The clinical presentation is not specific and radiographs alone are often not diagnostic (*3*). Despite the development of new imaging modalities, the diagnosis of early bone infection remains elusive (*3,4,8,12,17*). If deep infection is suspected, confirmatory invasive procedures are indicated. Invasive or reoperative procedures, however, increase the likelihood of postoperative infection. Accurately ruling out the presence of infection, or predicting its cure, obviates further invasive procedures or expensive unnecessary antibiotics.

Staphylococcus aureus is the most common aerobic isolate from osteomyelitis in man and dogs (*1–3*). Seventy-five percent of osteomyelitis secondary to a contiguous focus of infection is related to fracture, with 60% related to surgical repair of fractures (*1,2*). Our model was selected to simulate a repaired fracture and was modified from previously reported methods (*26*). A cortical defect was created to stimulate a healing response and a foreign body was introduced to mimic surgical implants. Certainly, the cotton foreign body should be more reactive than most orthopedic implants.

Radiographs were not an accurate indicator of infec-

TABLE 3
Mean Values for Postoperative ^{99m}Tc-MDP and ^{111}In-Cl Scans

	Infected	Noninfected	p value
^{99m}Tc-MDP			
Tibia/Femur	2.19	1.88	0.0199
Tibia/Dist Tibia	7.07	6.03	0.2970
Tibia/Soft Tissue	25.64	13.33	0.0044
Femur/Soft Tissue	13.33	13.83	0.0570
^{111}In-Cl (24-hr)			
Tibia/Femur	1.93	1.32	0.0001
Tibia/Dist Tibia	4.21	3.54	0.0679
Tibia/Soft Tissue	3.75	2.10	0.1356
Femur/Soft Tissue	2.02	1.62	0.8101
^{111}In-Cl (72 hr)			
Tibia/Femur	2.04	1.30	0.0001
Tibia/Dist Tibia	4.74	3.19	0.0350
Tibia/Soft Tissue	3.89	2.53	0.0385
Femur/Soft Tissue	2.06	2.06	0.2765

TABLE 4
Infected/Noninfected Ratio

	24-hr			72-hr	
	^{99m}Tc-MDP	^{111}In-Cl	p value*	^{111}In-Cl	p value*
Day 5	1.27	1.38	0.18	1.48	0.03
Day 14	1.21	1.58	0.008	1.64	0.004
Day 23	1.46	1.62	0.09	1.76	0.42
Postop mean	1.31	1.53	0.01	1.62	0.002

* For difference between ^{99m}Tc-MDP and preceding ^{111}In-Cl value.

TABLE 5
Indium-111-Cl/^{99m}Tc-MDP Ratios

		Infected	Noninfected	p value
Day 5	24 hr	1.11	1.01	0.08
	72 hr	1.12	1.02	0.11
Day 14	24 hr	0.72	0.53	0.0015
	72 hr	0.75	0.51	0.003
Day 23	24 hr	0.68	0.59	0.27
	72 hr	0.67	0.52	0.066
Postop mean	24 hr	0.84	0.71	0.0009
	72 hr	0.85	0.68	0.0002

tion. On postoperative Day 5, radiographs were unable to predict infection. However, by Day 23 radiographs were reliable in identifying bone infection. Although radiographic findings of osteomyelitis are well established (*3,4*), differentiation of active from inactive disease by radiographic signs can be difficult (*3,13*). Initial radiographic signs may be subtle and nonspecific (*3,4*). A progression or regression of radiographic signs is frequently necessary to substantiate a diagnosis (*3*). Sites of radiographic abnormalities may not represent optimal biopsy sites because of the delay in radiographic changes. Detection of infection in patients with previous surgery or fracture is more difficult due to postoperative changes or fracture healing masking or mimicking the infectious process (*3,13*). In addition to being relatively insensitive, radiographs are a poor indicator of the course of disease. Often patients have radiographic signs of progressive disease while improving clinically (*2,3,13*).

A variety of nuclear medicine procedures have been investigated for detection of infection or inflammation in bone and other tissues. The ideal radiotracer for the in vivo localization of inflammation should:

1. Be highly specific for inflammatory lesions.
2. Accumulate rapidly at inflammatory foci.
3. Have low background activity.
4. Have gamma emission suitable for imaging with a scintillation camera.
5. Deliver a low patient-absorbed dose.
6. Be easy to prepare and administer (*13*).

TABLE 6
Sensitivity, Specificity, and Predictive Values for Region of Interest Ratios

	Cutoff	Sens	Spec	ppv	npv
^{99m}Tc-MDP					
Tibia/Femur	1.7	0.61	0.77	0.62	0.70
Tibia/Soft Tissue	1.0	0.60	0.57	0.48	0.68
^{111}In-Cl					
24-hr Tibia/Femur	1.6	0.61	0.88	0.75	0.79
72-hr Tibia/Femur	1.6	0.59	0.88	0.83	0.68
72-hr Tibia/Dist Tibia	4.25	0.62	0.69	0.67	0.65
72-hr Tibia/Soft Tissue	3.1	0.70	0.85	0.82	0.74

Since its introduction in 1971, ^{99m}Tc-MDP bone scintigraphy has been a valuable tool in detecting osteomyelitis and three-phase bone scanning has added to the specificity of the technique (*6*). While radionuclide bone imaging is superior to radiography for early detection of osteomyelitis, it is often difficult to separate osteomyelitis from nonosseus inflammatory disease (*4, 6*). In the presence of fracture or bone surgery, the diagnosis of infection is hindered. Some bone scans fail to become positive in osteomyelitis, possibly due to infarction or decreased blood supply (*13*).

Radionuclide angiograms add sensitivity (*14*) to the bone scan. While the postoperative radionuclide angiograms identified the infected limb in most image sets in our study, the validity is suspect because of the inexplicable positive preoperative studies. In another animal model, bone-phase images remained negative during the first 4 days after introduction of a pyogenic material, while angiogram phase images became positive on the second day (*14*).

In this study, blood-pool phase images were able to differentiate infected from noninfected limbs. In the absence of a sham-operated control limb for comparison, the ability to definitively diagnose infection would be unlikely. Likewise, the increased activity of the operative site versus the ipsilateral femur or soft tissues confirms the reported high sensitivity and low specificity of the technique.

Technetium-99m-MDP quantitative bone images were different for infected and noninfected limbs. Both T/F and tibia-to-soft tissue average ratios were increased in the infected limb. The large variability of individual values for both infected and noninfected bone made diagnostic use of this difference difficult. While all osseous lesions demonstrated increased ^{99m}Tc-MDP uptake and would not have been overlooked on subjective interpretation, a positive scan was defined as one where the region of interest ratio exceeded a given value. Using a optimum cutoff value of 1.7, the sensitivity and specificity of T/F ratios were 61% and 77%, respectively. Although not used in our study, 24-hr delayed bone images (four-phase bone scans) have been reported to improve the specificity of ^{99m}Tc-MDP bone scans (*15*).

Increased ^{99m}Tc-MDP localization is dependent on increased tracer delivery (blood flow) and increased tissue extraction (increased capillary permeability, local extracellular fluid volume, or bone metabolism) (*11*). Technetium-99m-MDP uptake correlates best with the histologic finding of early mineralizing osteoid (*11*). Uptake of ^{99m}Tc-MDP stops at 4 hr in lamellar bone and 4–24 hr in woven bone (*15,27*). With bone infection, there is an increased amount of woven bone (as well as hyperemia) and uptake continues for 24 hr (*15, 27*). With soft-tissue infection adjacent to noninfected bone, hyperemia results in increased uptake. Twenty-

four-hour ^{99m}Tc-MDP images provide an increase in specificity but no increase in sensitivity (*15*).

Gallium-67-citrate scans are more specific than ^{99m}Tc-MDP (*4,5,8*) but some labeling of tumors (*4*), healing fractures (*4,5,8,28*), noninfected orthopedic implants (*4*), and previously treated (but culture negative) osteomyelitis (*9,28*) occurs. Additionally, there are technical problems associated with the physical and biologic characteristics of ^{67}Ga (*11*).

Indium-111- or ^{99m}Tc-labeled leukocytes remain the standard for imaging acute inflammation (*3,8*). However, false-positives occur with open fractures, some tumors, and synovitis (*3*). False-negatives may occur in chronic osteomyelitis with low numbers of granulocytes (*3,8*). There are technical problems associated with white cell labeling and imaging (*13*): long preparation time, poor spatial resolution, absence of bone landmarks on images, and confusing uptake in bone marrow regions.

In the early 1970s, ^{111}In-Cl was investigated for use in labeling tumors (*29–33*) and differentiating focal liver disease (*33,34*). While ^{111}In has more favorable physical characteristics, ^{67}Ga was found to be superior in identifying tumors. Indium-111-chloride was introduced for erythroid marrow scintigraphy in 1973 (*23*). Indium-111-chloride has been used as a noninvasive means of evaluating patients with marrow aplasia and myelofibrosis. There is a good correlation between ^{111}In-Cl uptake and the presence of erythroid marrow which aids in localization for marrow biopsy (*22*).

In previous clinical reports of ^{111}In-Cl scanning of infection, images have been considered positive if any uptake was present other than normal marrow (*18,29, 21*). In our experiment, there was increased activity at the operative site in both the infected and noninfected limbs. The presence of a foreign body was presumably responsible for the uptake in the noninfected limb, as an inflammatory reaction was noted on histologic examination of the implant site. Despite the superimposition of bone healing and foreign-body reaction, ^{111}In-Cl differentiated infected from noninfected sites ($p = 0.0001$).

Assigning a cutoff value for ^{111}In-Cl T/F ratios with reasonable sensitivity resulted in a 88% specificity for detecting infection in the face of bone healing and foreign-body reaction. The requirement for this level of sensitivity (66%) may be too stringent in fracture or surgical patients since the site of possible infection would be known. In a subjective evaluation of scans of clinical patients with hip prostheses, ^{111}In-Cl had a sensitivity of 86% and a specificity of 60% for detecting infection, while ^{99m}Tc-MDP was 100% sensitive and 0% specific (*21*). Those authors also concluded that ^{111}In-Cl and ^{67}Ga scanning have similar accuracy, but ^{111}In-Cl images were simpler to interpret since any increased uptake is abnormal (*21*). Indium-111-chloride has been used to detect rheumatoid arthritis with similar sensitivity (74%) and specificity (73%) (*24*). In those uncommon instances where bone scans are negative (very early disease, neonatal osteomyelitis), ^{111}In-Cl may prove useful in identifying foci of inflammation.

Twenty-four-hour ^{111}In-Cl images were diagnostic. Tibia/femur and In-Cl/Tc-MDP ratios did not significantly change by waiting 72 hr to image patients. The 10-hr plasma half-life of indium (*30,32*) results in greater tibia-to-soft tissue ratios on the later images. With ^{67}Ga, accumulation in tumor or abscess is nearly complete 2 hr after injection, but images are delayed 48 hr to decrease blood levels and thereby increase target-to-background contrast (*8*). In early tumor labeling studies, ^{111}In-Cl tumor-to-organ ratios were lower than those for ^{67}Ga (*30,33*).

Infected/noninfected ratios were greater for ^{111}In-Cl than ^{99m}Tc-MDP, presumably because of increased accumulation of inflammatory exudate in the infected site. Ratios may have been decreased by the presence of the cotton foreign body in the control limb.

Indium-chloride/Tc-MDP ratios were greater in the infected limb than the control limb. Little difference was observed between 24- and 72-hr ratios. Indium-111-chloride accumulation at sites of infection is, at least in part, due to mechanisms different from those of MDP.

Gallium and indium differ from ^{99m}Tc-MDP in their mechanism of localization and concentration in inflamed bone. When heat-killed *S. aureus* was injected into the tibias of rabbits, delayed ^{99m}Tc-MDP images on postinjection Days 1–4 had reduced uptake at the injection site, while ^{67}Ga scans during that time showed increased activity (*14*). Other studies have reported similar results with ^{67}Ga images that are positive early in infection and with ^{99m}Tc-MDP requiring 5–7 days to become positive (*7,16*). Gallium-67 localization is linked to serum protein exudation and in vivo labeling of leukocytes (*16*); ^{99m}Tc-MDP localization is related to increased flow and extraction.

Indium-chloride and gallium-citrate exhibit many similarities in distribution and localization within the body. After i.v. injection, ^{67}Ga and ^{111}In bind rapidly to transferrin (*35,36*), but clear rapidly from plasma (*13,31*). In animal models, ^{111}In-Cl identifies cells expressing transferrin receptors (*24*). Cells take up ^{111}In by receptor-mediated endocytosis (*37*). For localization, indium need not be released from protein but only leaked into the extravascular space (*37*). The increased vascular permeability and expanded extracellular fluid space observed at sites of inflammation are important in radionuclide localization (*38*). Transferrin is present in inflammatory lesions, but at a low concentration. Lactoferrin, secreted in lysosomes by stimulated or dead neutrophils, is present in high concentration (*38*). The transfer of indium from transferrin to tissue lactoferrin

or ferritin in an inflammatory focus is likely to cause sufficient radionuclide accumulation for gamma camera imaging (*13,38*). Phosphate compounds play a role in localization. Pyrophosphate may serve as a physiologic chelator, and increasing levels of ATP causes the transfer of indium from transferrin to ferritin (*37*). The influence of ^{99m}Tc-MDP on ^{111}In-Cl biodistribution has not been investigated but theoretically could decrease target-to-background contrast.

Indium-chloride may offer a method of evaluating the response of osteomyelitis to antibiotic therapy through serial scintigraphic examinations. Technetium-99m-MDP, ^{111}In-labeled leukocytes, and ^{67}Ga have been reported to reflect the response of osteomyelitis to antibiotic therapy (*9,10,39*) but do not accurately predict the long-term results (*9,10,28,39,40*). In one study of 40 patients, ^{111}In-Cl accurately predicted the long-term outcome of therapy (*41*). In 26 individuals with normal scans, osteomyelitis did not recur. In seven patients with persistently abnormal scans, recurrence occurred in all within two years. Four patients had mild uptake associated with arthritis and three had persistent low-grade soft-tissue infection.

The major problem associated with ^{111}In-Cl imaging is separating bony involvement from adjacent soft-tissue infection. While the influence of view on ^{99m}Tc-MDP and ^{111}In-Cl bone images was not significant, its effect on the diagnostic accuracy of an individual scan must be considered. Indium-111-chloride proved an excellent agent for imaging both soft-tissue infection associated with the adjacent bone infection and the mild cellulitis associated with animals licking at the skin incision sites. In one study of over 250 patients with suspected inflammatory disease, ^{111}In-Cl was 92% sensitive and 95% specific (*20*). Just as ^{99m}Tc-MDP is not specific for the type of bone disease, ^{111}In-Cl is not specific for the site of infection. The combination of the ^{99m}Tc-MDP and ^{111}In-Cl scintigraphy holds future promise for the diagnosis of osteomyelitis. Parametric ratio imaging using simultaneous acquisition of ^{111}In-Cl and ^{99m}Tc-MDP images is currently under investigation for spontaneously occurring osteomyelitis.

Because of the high diagnostic sensitivity of ^{99m}Tc-MDP, immediate availability, low cost, high resolution, and short total scan time, it remains the first choice for diagnostic imaging in inflamed bone (*13*). Indium-111-chloride should be considered for confirmation of acute or chronic infection prior to more invasive diagnostics. It is particularly well suited for imaging in the face of known bone injury (fracture, surgery). Indium-111-chloride's promise as a predictor of therapeutic outcome is currently under investigation.

ACKNOWLEDGMENTS

A part of this work was reported at the 1989 meeting of the American College of Veterinary Radiology, Breckenridge, CO, August 16–19, 1989.

This project was funded partially by a Venture Grant from the Institute of Agriculture, University of Tennessee. Other support is from general research funds from the Department of Urban Practice, University of Tennessee.

The authors thank Mr. Paul Ollis, Ms. Samedi Piantidosi, Mr. Randy Juracek, Ms. Brenda Loveday, and Ms. Theresa Spiker for their assistance. Ms. Mary Jean Bryant provided the bacterial isolate and microbioligic support. The authors also thank Dr. William Sanders for his assistance with the statistical analysis.

REFERENCES

1. Caywood DD, Wallace LJ, Braden TD. Osteomyelitis in the dog: a review of 67 cases. *J Am Vet Med* 1978;172:973–946.
2. Waldfogel FA, Medoff G, Swartz MN. Osteomyelitis: a review of clinical features, therapeutic considerations and unusual aspects. *N Engl J Med* 1970;282:198–205,260–266,316–321.
3. Resnick D, Niwayama G. Osteomyelitis, septic arthritis, and soft tissue infection: the mechanism and situations. In: Resnick D, Niwayama G, eds. *Diagnosis of bone and joint disorders with an emphasis on articular abnormalities.* Philadelphia: WB Saunders; 1981:2042–2129.
4. Al-Sheikh W, Sfakianakis GN, Mnaymneh W, Hourani M, Heal A. Subacute and chronic bone infections: diagnosis using In-111, Ga-67, and Tc-99m-MDP bone scintigraphy, and radiography. *Radiology* 1985;155:501–506.
5. Lewin JS, Rosenfield NS, Hoffer PB, Dowining D. Acute osteomyelitis in children: combined Tc-99m and Ga-67 imaging. *Radiology* 1986;158:795–804.
6. Maurer AH, Chen DCP, Camargo EE, et al. Utility of three-phase skeletal scintigraphy in suspected osteomyelitis: concise communication. *J Nucl Med* 1981;22:941–949.
7. Dye SF, Lull RJ, McAuley RJ, et al. Time sequence of bone and gallium scan changes in acute osteomyelitis: an animal model [Abstract]. *J Nucl Med* 1979;20:647.
8. Schauwecker DS, Park HM, Mock BH, et al. Evaluation of complicating osteomyelitis with Tc-99m-MDP, In-111-granulocytes, and Ga-67-citrate. *J Nucl Med* 1984;25:849–853.
9. Graham GD, Lundy MM, Moreno AJ, Frederick RJ. The role of Tc-99m-MDP and Ga-67-citrate in predicting the cure of osteomyelitis. *Clin Nucl Med* 1983;5:344.
10. Tumeh SS, Aliabadi P, Weissman BN, McNeil BJ. Chronic osteomyelitis: bone and gallium scan patterns associated with active disease. *Radiology* 1986;158:685–688.
11. Kirchner PT, Simon MA. Current concepts review: radioisotope evaluation of skeletal disease. *J Bone Joint Surg* 1981;63:673–681.
12. Beltran J, McGhee RB, Shaffer PB, et al. Experimental infection of the musculoskeletal system: evaluation with MR imaging and Tc-99m-MDP and Ga-67-scintigraphy. *Radiology* 1988;167:167–172.
13. Kim EE, Haynie TP, Podoloff DA, Lowry PA, Harle TS. Radionuclide imaging in the evaluation of osteomyelitis and septic arthritis. *Crit Rev Diag Imaging* 1989;29:257–305.
14. Norris SH, Watt I. Radionuclide uptake during the evolution of experimental acute osteomyelitis. *Br J Radiol* 1981;54: 207–211.
15. Israel O, Gips S, Jerushalmi J, Frenkel A, Front D. Osteomyelitis and soft-tissue infection: differential diagnosis with 24-hour/4-hour ratio of Tc-99m-MDP uptake. *Radiology* 1987;163:725–726.
16. Hartshorne MF, Graham G, Lanaster T, Berger D. Gallium-67/Technetium-99m-methylene diphosphonate ratio imaging: early rabbit osteomyelitis and fracture. *J Nucl Med* 1985;26:272–277.

17. Sandler MP, Stein S, Holburn G, Partain CL. Comparison of Ga-67 scintigraphy and contrast-enhanced MR imaging in early diagnosis of acute staphylococcal induced osteomyelitis in a rabbit model. Presented at the 72nd Scientific Assembly and Annual Meeting of the Radiological Society of North America, Chicago, Nov 30, 1986.
18. Iles SE, Ehrlick LE, Saliken JC, Martin RH. Indium-111-chloride scintigraphy in adult osteomyelitis. *J Nucl Med* 1987;28:1540–1545.
19. Sayle BA, Fawcett HD, Wilkey DJ, et al. Indium-111-chloride imaging in chronic osteomyelitis. *J Nucl Med* 1985;26:225–229.
20. Sayle BA, Balachandran S, Rogers CA. Indium-111-chloride imaging in patients with suspected abscesses: concise communication. *J Nucl Med* 1983;24:1114–1118.
21. Sayle BA, Fawcett HD, Wilkey DJ, Gierny G, Mader JT. Indium-111-chloride imaging in the detection of infected prostheses. *J Nucl Med* 1985;26:718–721.
22. Gilbert EH, Earle JD, Goris ML, Kaplan HS, Kriss JP. The accuracy of ^{111}In-Cl_3 as a bone marrow scanning agent. *Radiology* 1976;119:167–168.
23. Lillien DL, Berger HG, Anderson DP, et al. Indium-111-chloride: a new agent for bone marrow imaging. *J Nucl Med* 1973;14:184–186.
24. Schmerling RH, Parker JA, Johns WD, Trentham DE. Indium-111-chloride joint imaging in rheumatoid arthritis [Abstract]. *J Nucl Med* 1989;30:885.
25. Abdel-Dayem HM, Breen J, Leslie EV. Clinical experience with [^{111}In]indium chloride scanning in inflammatory diseases. *Clin Nucl Med* 1978;5:196–201.
26. Fitzgerald RH. Experimental osteomyelitis: description of a canine model and the role of depot administration of antibiotics in the prevention and treatment of sepsis. *J Bone Joint Surg* 1983;65:371–380.
27. Arnold JS. Mechanism of fixation of bone imaging radiopharmaceuticals. In: Billinghurdt ME, ed. *Studies of cellular function using radiotracers.* Boca Raton: CRC Press; 1980:115–144.
28. Alazraki N, Fierer J, Resnick D. Chronic osteomyelitis: monitoring by ^{99m}Tc-phosphate and ^{67}Ga-citrate imaging. *AJR* 1985;145:767–771.
29. Hunter WW, Riccobono XJ. Clinical evaluation of ^{111}In for localization of recognized neoplastic disease. *J Nucl Med* 1970;11:328.
30. Goodwin DA, Imbornone CJ, Song CH. Comparative study of tumor and organ distribution of ^{111}In- and ^{67}Ga-labeled compounds in mice. *J Nucl Med* 1971;12:434.
31. Goodwin DA, Goode R, Brown L, Imbornone CJ. Indium-111-labeled transferrin for the detection of tumors. *Radiology* 1971;100:175–179.
32. Farrer PA, Saha GB, Shibata HN. Evaluation of ^{111}In-transferrin as a tumor scanning agent in humans. *J Nucl Med* 1972;13:429.
33. Lomas F, McKusick KA, Dibos PE, Wagner HN. Ionic ^{67}Ga and ^{111}In in the differential diagnosis of focal liver disease. *J Nucl Med* 1972;13:450.
34. Abdel-Dayem HM, Elkousy AM, Leslie EV, Panaro VA. Experience with ^{111}In-chloride scanning in patients with focal defects on ^{99m}Tc-sulfur colloid liver scans. *Radiology* 1975; 114:403–406.
35. Stern HS, Goodwin DA, Scheffel U, et al. Indium-113 for blood pool and brain scanning. *Nucleonics* 1967;25:62–65.
36. Ito Y, Okayama S, Sato K, et al. Gallium-67 tumor scanning and its mechanisms studied in rabbits. *Radiology* 1971;100: 357–362.
37. Weiner RE. Role of phosphate-containing compounds in the transfer of indium-111 and gallium-67 from transferrin to ferritin. *J Nucl Med* 1989;29:70–79.
38. Tsan MF. Mechanism of gallium-67 accumulation in inflammatory lesions. *J Nucl Med* 1985;26:88–92.
39. Graham GD, Lundy MM, Frederick RJ, et al. Predicting the cure of osteomyelitis under treatment: concise communication. *J Nucl Med* 1983;24:110–113.
40. Wagner DK, Collier BD, Rytel MW. Long-term intravenous antibiotic therapy in chronic osteomyelitis. *Arch Int Med* 1985;145:1073–1078.
41. Sayle BA, Mader JT, Cierny G. Indium-111-chloride imaging in treated osteomyelitis [Abstract]. *J Nucl Med* 1988;29:763.